Polarization, energetics, and electrorheology in carbon nanotube suspensions under an applied electric field: An exact numerical approach

Amir A. Farajian,[1,*] Olga V. Pupysheva,[1] Howard K. Schmidt,[2] and Boris I. Yakobson[1,3]
[1]*Department of Mechanical Engineering and Materials Science, Rice University, Houston, Texas 77005, USA*
[2]*Carbon Nanotechnology Laboratory, Rice University, Houston, Texas 77005, USA*
[3]*Department of Chemistry, Rice University, Houston, Texas 77005, USA*
(Received 19 June 2007; revised manuscript received 21 April 2008; published 22 May 2008)

We theoretically investigate the polarization, aggregation, and yield stress in carbon nanotube suspensions under an electric field. The nanotubes are modeled as solid rods with hemispherical ends. An exact numerical approach, which includes self-consistent Coulomb interactions within classical electrostatics, is employed to derive nanotube surface charge densities. Two essential nanotube characteristics, i.e., large aspect ratios and end contributions, are included together. The reliability of the model is demonstrated by comparing the calculated emerging yields against experimental data. The onsets of system parameters can be used to control the phase transition in nanotube suspensions.

DOI: 10.1103/PhysRevB.77.205432 PACS number(s): 61.46.Fg, 65.80.+n, 83.80.Hj, 47.65.Gx

I. INTRODUCTION

The unique characteristics of carbon nanotubes, i.e., their size, aspect (length to diameter) ratio, stiffness, and thermal, electronic, and transport properties, make nanotube suspensions attractive for various applications. These include nanotube-filled thermoplastic elastomers,[1] nanotube aerogels,[2] cancer therapy,[3] and fibers with anisotropic conduction.[4] In the specific case of liquid crystal suspensions, for example, carbon nanotubes are shown to align along a uniform liquid crystal director field,[5] with possible applications in magnetically steered electric switches.[6] Nanotubes have been used as fillers in the liquid crystal matrix[7] and are shown to control the field-off and field-on response times and threshold voltages of liquid crystals.[8] These effects may be applicable in liquid crystal displays.

The orientation and aggregation of the nanotubes strongly affect the properties of the suspension. Controlled phase transition in nanotube suspensions is therefore of great importance. One way to achieve phase transition is subjecting the suspensions to electric field or electromagnetic radiation (Fig. 1), which dramatically changes the suspension's viscoelastic response, among others. This response, i.e., the electrorheology[9] in nanotube suspensions, has been studied in recent experiments.[10–12]

A necessary issue in modeling nanotube suspensions under an applied electric field is the proper inclusion of the nanotubes' (longitudinal) polarizations. (For metallic nanotubes, whose response is dominant, transverse polarizations are negligible in comparison.) The standard model for electrorheological suspensions, which uses point dipole approximation,[13,14] cannot be used for nanotubes owing to their large aspect ratios. Other models of nanotube longitudinal polarizabilities usually neglect the end contributions.[15–17] Owing to computational limits, polarization models for entire nanotube (including its ends) that are capable of treating realistic aspect ratios have been rather rare.[18,19] For modeling the nanotubes' polarization, aggregation, and electrorheological behavior, including *both* large aspect ratios *and* end contributions, however, is essential.

Here, we present an exact self-consistent method, within classical electrostatics, to achieve this aim. The method is based on solving an integral equation for the (continuous) surface charge densities within a solid-rod model for the nanotubes, in which they are treated as solid cylindrical rods with hemispherical ends. The solid-rod model for nanotubes is justified by their large ($\sim$1.2 TPa) Young's modulus[20] and long ($\sim$0.1 mm) persistence length,[21] the latter being much larger than a typical nanotube's length. Although not as sophisticated as *ab initio*[17] or tight-binding[16,19] treatments, our approach has the advantage of including both large aspect ratios and end contributions. We calculate the onsets of system parameters for overcoming Brownian agitations. The calculated upper bounds for the yield stress of the organized phase of the suspensions agree well with the experimental results.

II. MODEL AND METHOD

For metallic and semiconducting nanotubes immersed in a nonconducting dielectric solution, the interfaces are of conductor-dielectric (CD) and dielectric-dielectric (DD) types, respectively. The discontinuity of electric displace-

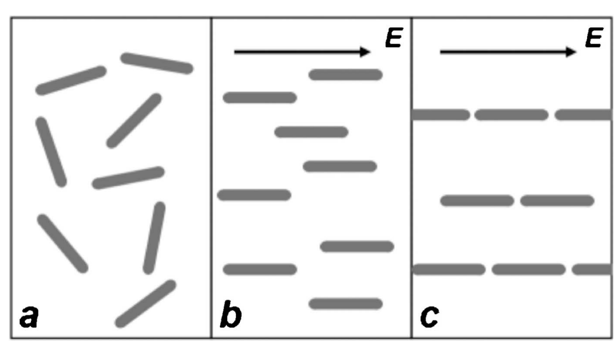

FIG. 1. Schematic of a dispersed solution of nanotubes (a). Upon application of an electric field, the nanotubes become polarized, align with the applied field (b), and subsequently aggregate in chainlike structures (c).

ment vector $\mathbf{D}=\varepsilon\mathbf{E}$ ($\mathbf{E}$ is the electric field) in the former case and its continuity in the latter are used to express the potential in terms of the total charge densities at the interfaces. These include the sum of the polarization and free charges for the CD interfaces and the polarization charges for the DD interfaces. By integrating the singularity that arises when the source and field points, $\mathbf{x}'$ and $\mathbf{x}$, coincide,[22] we obtain (in SI units)[23–27]

$$\sigma(\mathbf{x}) = 4\pi\varepsilon_0\lambda E_n(\mathbf{x}) - \lambda\sum_i \oint_{S_i,\mathbf{x}'\neq\mathbf{x}} \sigma(\mathbf{x}')\frac{\partial}{\partial n(\mathbf{x})}\left(\frac{1}{|\mathbf{x}-\mathbf{x}'|}\right)dS'. \tag{1}$$

Here, σ is the total charge density, ε_0 is the vacuum permittivity, and λ equals $1/2\pi$ and $(\varepsilon_s-\varepsilon_e)/2\pi(\varepsilon_s+\varepsilon_e)$ for the CD and DD interfaces, respectively, where ε_s and ε_e are the relative dielectric constants of the semiconducting nanotubes and the (solvent) environment. E_n is the normal component of the applied electric field, S_i is the surface of the ith nanotube, and $\partial/\partial n(\mathbf{x})$ indicates the derivative with respect to the normal direction to the surface at $\mathbf{x}$. We consider only dc external fields, or ac external fields with oscillation periods much larger than the nanotubes' response time, and ignore the frequency dependence of ε_s and ε_e. This assumption will be made clearer shortly, after calculating the charge separation in nanotubes under an electric field, which provides an estimate for the response time of the nanotubes.

Equation (1) is a Fredholm integral equation of the second kind and can be exactly solved by numerical discretization.[26,27] The proper treatment of the singularity at $\mathbf{x}'=\mathbf{x}$ is essential for accurate solutions, especially for nanotubes with large aspect ratios. We use qualocation discretization[28–30] with analytic integration over discrete panels[31] to ensure accuracy. This combination provides a very powerful solution strategy free from instabilities and divergences. As two simple tests, we checked that our calculated surface charge densities for a dielectric sphere and a rod (with the aspect ratio equal to 5) completely agree with other available calculations.[27,32]

III. RESULTS AND DISCUSSIONS

A. Surface charge density

We consider a dispersed and homogeneous nanotube solution and calculate the onsets of model parameters for overcoming thermal agitations of the solvent molecules such that the nanotubes get oriented parallel to the field. Assuming a single nanotube surface for Eq. (1), the surface charge densities are calculated for different radii and lengths. Figure 2(a) shows the induced surface charge densities for metallic nanotubes of different radii, but with a fixed stem length of 500 nm (excluding the ending hemispheres), parallel to an electric field of 1 kV/mm, which is a typical field used in experiments. We observe that the surface charge densities peak out at the ending hemispheres, especially for larger aspect ratios. Although the surface charge density at any longitudinal coordinate decreases by increasing the radius [Fig. 2(a)], one should notice that the linear charge density increases. Figure 2(b) shows that at points far enough from the

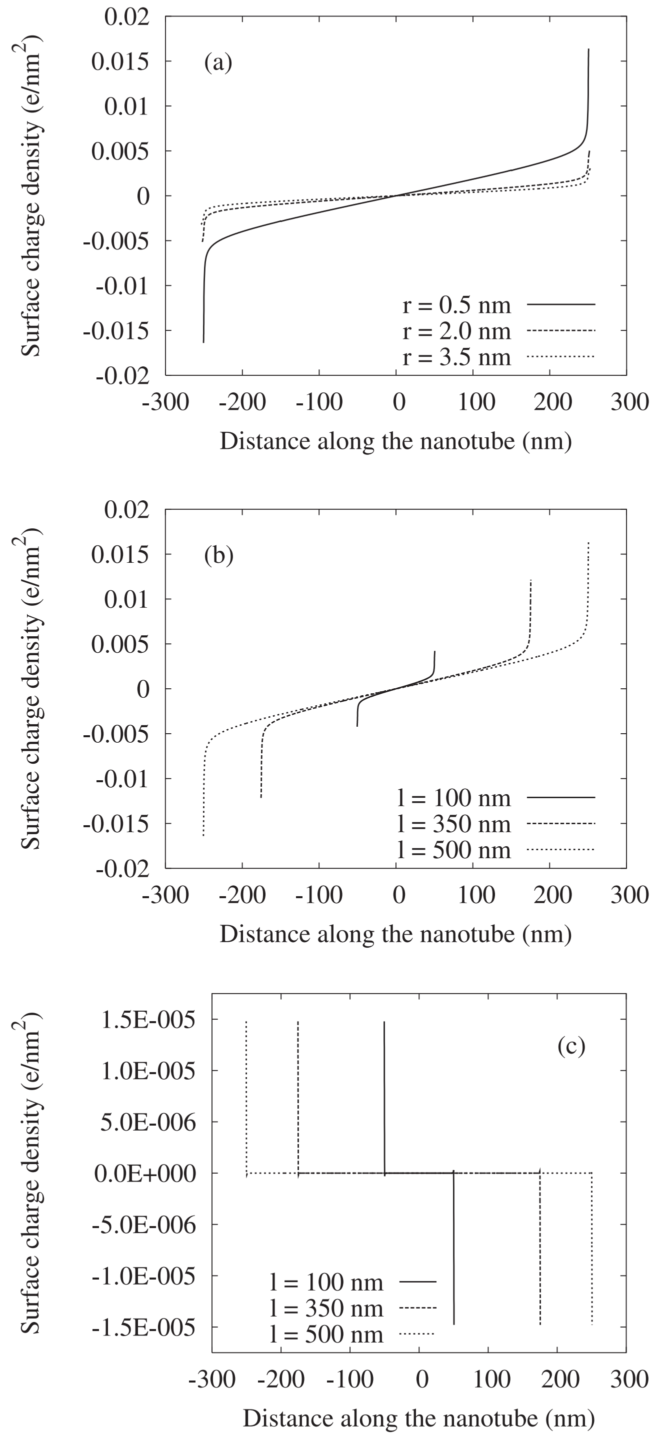

FIG. 2. Surface charge density along metallic nanotubes with different radii (a). The nanotube stems (excluding the ending hemispheres) extend from −250 to 250 nm. Surface charge density along metallic (b) and semiconducting (c) nanotubes with different stem lengths and a fixed radius of 0.5 nm. The applied electric field of 1 kV/mm is parallel to the nanotube's axis, and the solvent for semiconducting nanotubes is water.

ends, the charge density linearly increases along the nanotubes. This is in complete quantitative agreement with the analytic model that ignores the end contributions.[33] Near the ends, however, the charge density deviates from this linear

TABLE I. Values of $\gamma = pE/2kT$ for semiconducting (s) and metallic (m) nanotubes with different stem lengths and radii at $T=300$ K and $E=1$ kV/mm. The field-orientation domain is highlighted by the boldface numbers.

Stem length (nm)	$r_s=0.5$ nm (in water)	$r_s=0.5$ nm (in silicone oil)	$r_m=0.5$ nm	$r_m=2.0$ nm	$r_m=3.5$ nm	$r_m=5.0$ nm
100	0.2×10^{-4}	16.9×10^{-4}	0.16	0.28	0.38	0.48
350	0.7×10^{-4}	60.6×10^{-4}	**4.96**	**7.21**	**8.76**	**10.13**
500	1.1×10^{-4}	86.8×10^{-4}	**13.37**	**18.86**	**22.46**	**25.55**

dependence. Figure 2(b) shows that near the ends, the charge density satisfies another linear relationship with the length, i.e., with another proportionality constant.

Figure 2(c) shows the charge densities of semiconducting nanotubes with different stem lengths but with a fixed radius of 0.5 nm. For the semiconducting nanotubes, the permittivity $\varepsilon_s=60$ is used, which is a typical estimate to the low-frequency limit of the real part of the dielectric function observed in experiments.[34] For the solvent environment, we consider water with $\varepsilon_e=80$ as well as silicone oil[10–12] with $\varepsilon_e=2.75$,[35] whose density is very close to that of water. Comparing Figs. 2(c) and 2(b), we notice that the charge density of the semiconducting nanotubes is independent of the nanotube's length, localized at the ending hemispheres, and around 3 orders of magnitude less than the charge density of the metallic nanotubes. The signs of the ending charge densities of the semiconducting and the metallic nanotubes are opposite, which is due to the fact that the dielectric constant of the solvent environment is larger than that of the semiconducting nanotubes. The fact that metallic nanotubes have an infinite effective permittivity[36] makes them categorically different from semiconducting nanotubes, whose permittivity may vary but within a limited range (in comparison to the infinite permittivity of metallic nanotubes).

In reality, in addition to purely metallic and semiconducting nanotubes, "mixed" multiwall nanotubes that contain both metallic and semiconducting shells may exist. The response of such mixed multiwall nanotubes will be dominated by that of the metallic shell with the largest radius. Mixed multiwall nanotubes will therefore behave as metallic. For the case wherein the dominant metallic shell of a mixed multiwall nanotube is embedded in one or more semiconducting shells, two basic surfaces with an induced charge would exist: the surface of the dominant metallic shell and the overall outer (semiconducting) surface of the multiwall nanotube. Both of the corresponding surface charge densities can be calculated within our formalism; however, for simplicity, here we assume that the dominant metallic shell of a mixed multiwall nanotube is its outer shell.

Our choice of hemispherical ends for the nanotubes is justified by the fact that such capped nanotubes are the usual ones experimentally observed. In fact, hemispherical caps are energetically more stable compared to, e.g., "flat" caps. From the computational point of view, Sanchis *et al.*[27] showed that the flat ends for particles with smaller aspect ratios result in the singularity of the charge density, and hence the electric field, at the edges of the particle ends. This causes the interparticle forces to be larger than those calculated for hemispherical ends. The forces for these two types of endings, however, are of the same order of magnitude.[27] We therefore do not expect our results for the internanotube forces and yield stress (to be calculated shortly) to qualitatively change upon switching between these two types of endings. As the hemispherical caps correspond to physically observed nanotubes, here we consider only this type of ending.

B. Energetics of field alignment

By using the calculated charge densities, the nanotube dipole moment p is readily obtained. The parameter that determines the relative strength of the alignment energy as compared to the Brownian agitations is[37] $\gamma = pE/2kT$, where k is the Boltzmann factor and T is the absolute temperature. For $\gamma \gg 1$, the electric field overcomes the Brownian forces and effectively aligns the nanotubes, as depicted in Fig. 1(b).

Table I shows that for both metallic and semiconducting nanotubes, γ increases with length l. For the semiconducting nanotubes, the alignment energy is proportional to l because charges are induced only at the ends. For the metallic nanotubes, the growth of energy is much steeper and closer to be proportional to l^3, which is predicted by the analytic solution without end contributions.[33] This can be used to estimate the onset of the aligning field for which $E_{\mathrm{align}}^2 l^3 \propto kT$, giving $E_{\mathrm{align}} \propto \sqrt{T/l^3}$. Our results, however, are more precise because we exactly account for the end contributions.

The γ values for the semiconducting nanotubes are around 2–5 orders of magnitude less than those of the corresponding metallic nanotubes. Therefore, for the rest of this study, only metallic nanotubes are considered. One should notice, however, that for small-gap semiconducting nanotubes, the gap might possibly be closed at large enough temperatures. Such nanotubes should indeed be considered metallic.

Previous works on the properties of suspensions of long nanoparticles, such as the tobacco mosaic virus[37] and gold nanorods,[38] differ from ours in that they did not calculate the polarizability of their nanoparticles (whose aspect ratios are much smaller than that of the nanotubes considered here). In their models, they consider polarizability as a parameter that can be extracted from experimental data. They model the electro-optical properties of the suspensions and are not concerned with aggregation and chaining, which crucially depend on interparticle forces. For nanotubes with large aspect ratios, the end contributions play a significant role in internanotube forces. Within our approach, we are able to calculate the polarizations and forces, including the end contributions. This enables us to model the chaining of nanotubes and its byproducts such as electrorheology.

C. Energetics of chaining

After alignment with the applied field [Fig. 1(b)], chaining of the nanotubes occurs [Fig. 1(c)] provided that their interaction energy overcomes the Brownian agitation. A typical nanotube concentration in the suspensions used in experiments is 0.01 wt %.[10,12] In water or silicone oil, this implies 5×10^6 carbon atoms per μm^3. We consider multiwall armchair nanotubes with an outer-shell radius of 5 nm and a van der Waals distance of 0.35 nm between neighboring inner shells as an example. These nanotubes have roughly 2100 carbon atoms per unit cell. In a homogeneous suspension of such nanotubes with a length of 350 nm[11], the distance between the neighboring nanotubes both along their axis and perpendicular to it is a few hundreds nanometers.

We consider five nearest neighbor nanotubes that are aligned along a common axis for calculating the charge densities. The charge density of the middle one, together with that of a shifted replica, are then used for the rest of the calculations. (We checked that modeling an infinite chain of nanotubes with five nearest neighbors is enough to ensure relative errors in energies and forces between the middle nanotube and its shifted replica to be less than ~2%.) The Coulomb attraction potential energy U between two such nanotubes with radii of 5 nm, lengths of 350 nm, and an end-to-end intertube distance of 100 nm is obtained, by using the calculated charge densities under an applied field of 1 kV/mm, to be 31% of the thermal energy kT at room temperature. If the distance between the two ends of these nanotubes is the van der Waals distance of 0.35 nm, however, the Coulomb attraction is 15 times larger than the thermal energy. Considering the Coulomb repulsion between nearby parallel nanotubes, thermal agitations eventually result in chain formation, which constitutes a lower energy state of the system. The potential energies for different nanotubes and internanotube distances are compared to kT (T=300 K) in Fig. 3(a).

D. Interaction force and charge separation

The attractive force acting between any nanotube-replica pair i and j, which has been introduced above, is obtained as

$$F = \frac{1}{8\pi\varepsilon_0}\oint_{S_i}\oint_{S_j}\sigma(\mathbf{x})\sigma(\mathbf{x}')\frac{\hat{\mathbf{z}}\,.\,\hat{\mathbf{r}}}{|\mathbf{x}-\mathbf{x}'|^2}dSdS'. \qquad (2)$$

Here, $\hat{\mathbf{r}}$ and $\hat{\mathbf{z}}$ are the unit vectors along $\mathbf{x}-\mathbf{x}'$ and the common axis of the nanotubes, respectively. In Eq. (2), the charge densities are self-consistently calculated for each internanotube distance. We calculate the internanotube forces for a uniaxial chain of nanotubes subject to an electric field of 1 kV/mm. The results are depicted in Fig. 3(b). As expected, decreasing the internanotube distances results in a stronger Coulomb force. What prevents the nanotubes from getting connected is either the polymer wrapping or simply the repulsive van der Waals force.

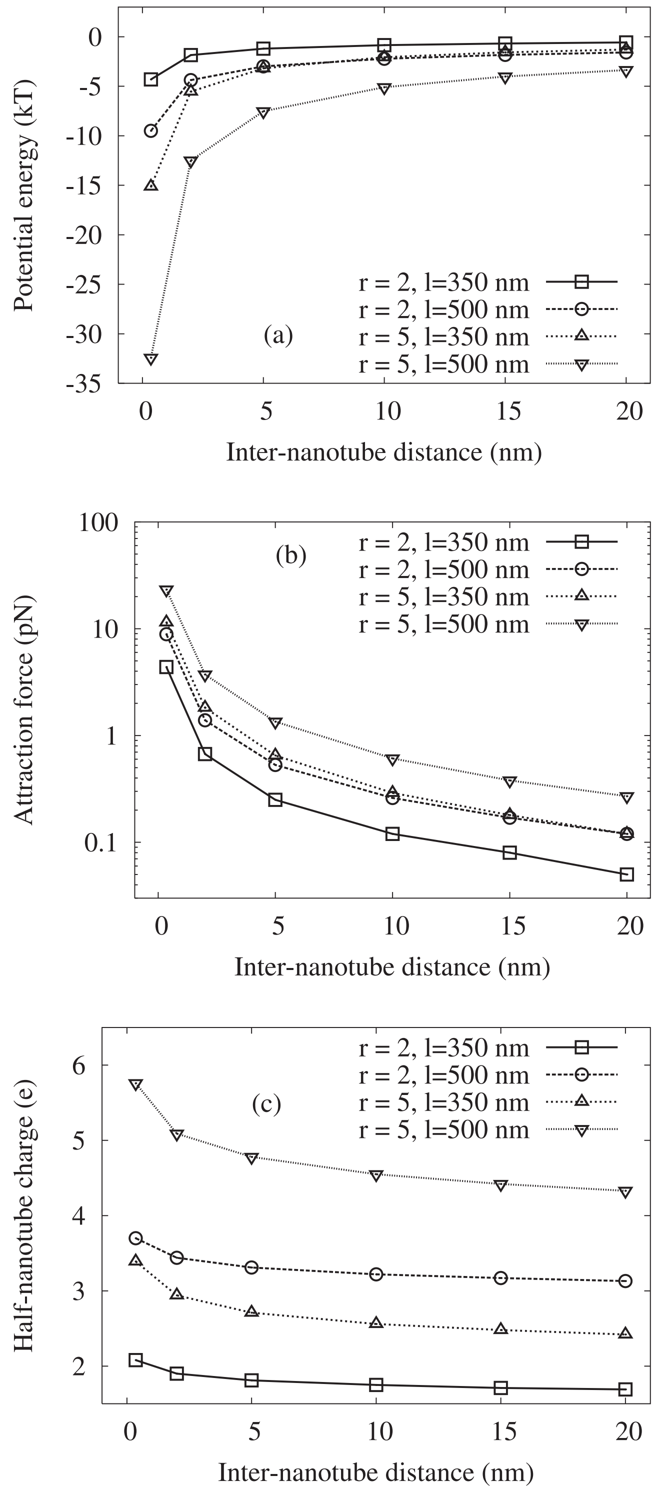

FIG. 3. Pair interaction potential (in units of kT with T=300 K) (a), attractive internanotube force (b), and the (continuous) half-nanotube charge (c) for different internanotube distances in an aggregated chain. The applied electric field is fixed at 1 kV/mm.

It is possible to interpret Eq. (2) in terms of the Maxwell stress tensor.[39] Here, as we are concerned with the mutual forces acting between separate conductors, the surface elements belong to different (neighboring) nanotubes.

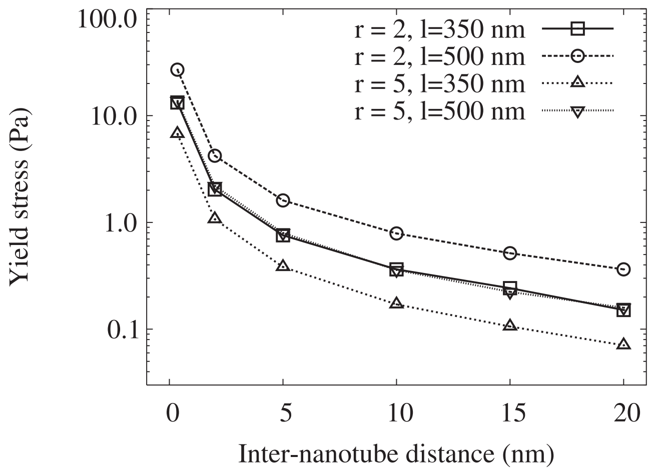

FIG. 4. Upper bounds for the yield stress in nanotube solutions consisting of different nanotube chains under a fixed electric field of 1 kV/mm.

When the nanotubes are polarized and aggregated as chains under the electric field, charge separation occurs within each nanotube. Therefore, for each nanotube, although the total charge is zero, each half would have a net charge that is opposite to the net charge of the half of the nearest neighboring nanotube in the chain. This charge separation is the basis of the interaction force. The net half-nanotube charges are depicted in Fig. 3(c). Although net charges differ for different nanotubes, Figs. 3(a) and 3(b) show that increasing the nanotubes' radii 2.5 times has essentially the same effect on energies and forces as increasing their lengths ~1.4 times.

E. Response time

Here, we use a simple model to estimate the response time $\tau = RC$, where R is the quantum resistance,[40] and we assign an effective capacitance $C = Q/V$ to the polarized nanotube. Here, Q and V indicate the half-nanotube charge and the applied potential drop, respectively.

For metallic nanotubes suspended in solution, the "contact" resistance[40] does not apply. However, the nanotubes may have defects, and there are electron-phonon (e-ph) scatterings at finite temperatures. The number of defects is roughly proportional to the length of the nanotube. If we assume that each defect (say, a vacancy) results in the suppression of one conduction channel of the nanotube,[41,42] we can assign a resistance of ~12.9 kΩ to each defect. It should be mentioned that resistances of this order are measured in experiments on individual multiwall nanotubes.[43] These resistances will be additive provided that there is a mechanism of dephasing (presumably including the e-ph interactions and/or solvent molecules) between successive scatterings of the carriers at different defects. By using the data of charge separation in Fig. 3(c) for a nanotube with a radius of 2 nm, a length of 350 nm, and an internanotube distance of 3.5 Å under an electric field of 1 kV/mm, for example, the capacitance is derived to be 9.1×10^{-19} F. Assuming one defect for the nanotube, the response time would be ~11.7 fs.[44] Therefore, in addition to the dc applied field, our results are valid for ac applied fields whose frequencies are much smaller than ~85 THz, i.e., are roughly on the order of terahertz or less. Interestingly, our estimate for the upper bound of the frequency is on the same order of magnitude as typical plasma frequencies of carbon nanotubes.[45–47]

The estimation in this section is based on one single defect of a specific type (a vacancy). This estimate, however, can be generalized to any other type/number of "defects," such as e-ph scatterings, whose resistance can be assessed.

F. Yield stress

The force data determines the rupturing tension[48] at different internanotube distances for separating neighboring nanotubes of a chain along their common axis. As other breaking routes, e.g., perpendicular to the chain axis, require less force, the force data in Fig. 3(b) can be used to estimate the upper bounds for the yield stress[49] of different nanotube chains. A nanotube concentration of 0.01 wt % in water or silicone oil implies effective cross sectional areas of 1.7×10^6 and 3.3×10^5 nm^2 for multiwall nanotubes with radii of 5 and 2 nm, respectively (the latter has roughly 420 carbon atoms per unit cell). This is based on the assumption that the internanotube distances are much smaller than their lengths. Dividing the forces by these effective cross sectional areas results in the yield-stress upper-bound data depicted in Fig. 4. Typical experimental values of the shear stress at low shear rates (which provide estimates of values for the yield stress) are few tenths to few tens pascals for a field strength of 1 kV/mm.[10–12] The results depicted in Fig. 4 very well correlate with these experimental values provided that the internanotube distances are less than 20 nm.

In order to see the importance of an accurate self-consistent calculation of surface charge density, we compare our results to those of the analytic solution for "endless" nanotubes. Assuming a linear induced charge density along the (metallic) nanotubes, in accordance with the available analytic model[33] and extending this assumption to the ending caps, one can estimate the resulting internanotube forces. We have performed such an estimate for nanotubes with $r = 2$ nm, $l = 350$ nm, and an internanotube distance of 0.35 nm as an example. The augmented linear model (with caps included) estimates the internanotube force to be 0.08 pN. Our self-consistent, nonlinear charge densities result in an internanotube force, which is depicted in Fig. 3(b), equal to 4.38 pN. Therefore, there is almost 2 orders of magnitude difference between the results of the augmented linear model and the accurate self-consistent calculations. It is thus clear that the aforementioned agreement between our results and the experimental data would not have been achieved had we used the augmented linear model, not to mention the nonaugmented one.

G. Field onsets for alignment and chaining

Owing to Eq. (1), the charge densities are linearly proportional to the applied field E. The γ values and the internanotube energies and forces are therefore proportional to E^2. The field onsets E_{align} and E_{chain} for alignment and chain formation are defined by $\gamma=1$ and $U=kT$, respectively. E_{align} and E_{chain} (in kV/mm) can thus be easily obtained as the inverse square roots of the γ and (the absolute value of) U given in Table I and Fig. 3(a), respectively. For example, with $r=2$ and $l=500$ nm, we obtain $E_{align}=0.23$ kV/mm, and with the internanotube distances equal to 2 nm, we get $E_{chain}=0.48$ kV/mm. Thus, for this configuration, the electric field is needed to be almost doubled to get the chains formed, after the alignment of the nanotubes.

The derivation of E_{chain} explained above is for a chain of nanotubes aligned with an applied field. If the applied field is less than E_{align} and, as a result, the nanotubes are prone to randomly agitate owing to thermal energy, a state of persistent polarization will not exist. As persistent polarization is a prerequisite for chain formation, we should discard E_{chain} if $E_{chain} < E_{align}$.[50]

IV. CONCLUSIONS

In conclusion, we analyze the polarization, aggregation, and electrorheology in nanotube suspensions under an electric field based on a numerically exact method. Estimates of the upper bounds for yield stress are shown to agree well with experimental results. We provide an estimate for the response time of the nanotubes and calculate the range of applied field frequencies for which the response time can be considered negligible. The field onsets for two levels of organization (alignment and chaining) are calculated for various system specifications. These onsets control the phase transition in nanotube suspensions, with exceptional application possibilities due to the unique characteristics of the constituting nanotubes.

ACKNOWLEDGMENTS

This work was performed under NASA Contract No. NNJ05HE75A through a subcontract from University of Texas Health Science Center. A. A. F. and B. I. Y. additionally acknowledge support from NSF NIRT Grant No. CMMI 0708096. We thank K. Esfarjani and A. Sadrzadeh for fruitful discussions.

*Present address: Department of Mechanical and Materials Engineering, Wright State University, Dayton, OH 45435; amir.farajian@wright.edu

[1] H. Koerner, G. Price, N. A. Pearce, M. Alexander, and R. A. Vaia, Nat. Mater. **3**, 115 (2004).
[2] M. B. Bryning, D. E. Milkie, M. F. Islam, L. A. Hough, J. M. Kikkawa, and A. G. Yodh, Adv. Mater. (Weinheim, Ger.) **19**, 661 (2007).
[3] Z. Liu, W. Cai, L. He, N. Nakayama, K. Chen, X. Sun, X. Chen, and H. Dai, Nat. Nanotechnol. **2**, 47 (2007).
[4] Y. Yamamoto, T. Fukushima, W. Jin, A. Kosaka, T. Hara, T. Nakamura, A. Saeki, S. Seki, S. Tagawa, and T. Aida, Adv. Mater. (Weinheim, Ger.) **18**, 1297 (2006).
[5] I. Dierking, G. Scalia, and P. Morales, J. Appl. Phys. **97**, 044309 (2005).
[6] I. Dierking and S. E. San, Appl. Phys. Lett. **87**, 233507 (2005).
[7] V. Weiss, R. Thiruvengadathan, and O. Regev, Langmuir **22**, 854 (2006).
[8] C.-Y. Huang, H.-C. Pan, and C.-T. Hsieh, Jpn. J. Appl. Phys., Part 1 **45**, 6392 (2006).
[9] T. C. Halsey, Science **258**, 761 (1992).
[10] H. J. Choi, S. J. Park, S. T. Kim, and M. S. Jhon, Diamond Relat. Mater. **14**, 766 (2005).
[11] S. J. Park, S. Y. Park, M. S. Cho, H. J. Choi, and M. S. Jhon, Synth. Met. **152**, 337 (2005).
[12] S. J. Park, M. S. Cho, S. T. Lim, H. J. Choi, and M. S. Jhon, Macromol. Rapid Commun. **26**, 1563 (2005).
[13] P. M. Adriani and A. P. Gast, Phys. Fluids **31**, 2757 (1988).
[14] R. T. Bonnecaze and J. F. Brady, J. Chem. Phys. **96**, 2183 (1992).
[15] E. G. Mishchenko and M. E. Raikh, Phys. Rev. B **74**, 155410 (2006).
[16] L. X. Benedict, S. G. Louie, and M. L. Cohen, Phys. Rev. B **52**, 8541 (1995).
[17] B. Kozinsky and N. Marzari, Phys. Rev. Lett. **96**, 166801 (2006).
[18] X. Zheng, G. H. Chen, Z. Li, S. Deng, and N. Xu, Phys. Rev. Lett. **92**, 106803 (2004).
[19] A. Mayer, Phys. Rev. B **71**, 235333 (2005).
[20] E. W. Wong, P. E. Sheehan, and C. M. Lieber, Science **277**, 1971 (1997).
[21] B. I. Yakobson and L. S. Couchman, J. Nanopart. Res. **8**, 105 (2006).
[22] R. Kress, *Linear Integral Equations*, 2nd ed. (Springer-Verlag, Berlin, 1999), pp. 78–82.
[23] J. Tausch and J. White, Adv. Comput. Math. **9**, 217 (1998).
[24] H. H. Pham and A. Nathan, IEEE Trans. Comput.-Aided Des. **18**, 1435 (1999).
[25] J. Tausch and J. White, IEEE Trans. Microwave Theory Tech. **47**, 18 (1999).
[26] M. Sancho, G. Martínez, and C. Martín, J. Electrost. **57**, 143 (2003).
[27] A. Sanchis, M. Sancho, G. Martínez, J. L. Sebastián, and S. Muñoz, Colloids Surf., A **249**, 119 (2004).
[28] Y. Massoud, J. Wang, and J. White, Technical Proceedings of the 1999 International Conference on Modeling and Simulation of Microsystems, 1999 (unpublished), p. 151.
[29] J. Tausch, J. Wang, and J. White, IEEE Trans. Comput.-Aided Des. **20**, 1398 (2001).
[30] M. D. Altman, J. P. Bardhan, J. K. White, and B. Tidor, Proceedings of the 2005 IEEE Engineering in Medicine and Biology 27th Annual Conference, 2005 (unpublished), p. 7591.
[31] J. N. Newman, J. Eng. Math. **20**, 113 (1986).
[32] J. D. Jackson, *Classical Electrodynamics*, 3rd ed. (Wiley, New York, 1999), p. 158.
[33] L. D. Landau, E. M. Lifshitz, and L. P. Pitaevskiĭ, *Electrodynamics of Continuous Media*, 2nd ed. (Butterworth-Heinemann, Washington, DC, 1984), p. 17.
[34] C. A. Grimes, E. C. Dickey, C. Mungle, K. G. Ong, and D. Qian, J. Appl. Phys. **90**, 4134 (2001).

[35] Y. C. Lan, S. Q. Men, X. Y. Xu, and K. Q. Lu, J. Phys. D: Appl. Phys. **33**, 1239 (2000).
[36] L. D. Landau, E. M. Lifshitz, and L. P. Pitaevskiĭ, *Electrodynamics of Continuous Media* (Ref. 33), p. 37.
[37] C. T. O'Konski, K. Yoshioka, and W. H. Orttung, J. Phys. Chem. **63**, 1558 (1959).
[38] B. M. I. van der Zande, G. J. M. Koper, and H. N. W. Lekkerkerker, J. Phys. Chem. B **103**, 5754 (1999).
[39] L. D. Landau, E. M. Lifshitz, and L. P. Pitaevskiĭ, *Electrodynamics of Continuous Media* (Ref. 33), p. 29.
[40] S. Datta, *Electronic Transport in Mesoscopic Systems* (Cambridge University Press, Cambridge, 1995).
[41] L. Chico, L. X. Benedict, S. G. Louie, and M. L. Cohen, Phys. Rev. B **54**, 2600 (1996).
[42] L. Chico, L. X. Benedict, S. G. Louie, and M. L. Cohen, Phys. Rev. B **61**, 10511 (2000).
[43] K. Mølhave, S. B. Gudnason, A. T. Pedersen, C. H. Clausen, A. Horsewell, and P. Bøggild, Nano Lett. **6**, 1663 (2006).
[44] Compare this to the response time of a doped nanotube junction, which is ~0.2 fs, K. Esfarjani, A. A. Farajian, Y. Kawazoe, and S. T. Chui, J. Phys. Soc. Jpn. **74**, 515 (2005).
[45] F. Bommeli, L. Degiorgi, P. Wachter, W. S. Bacsa, W. A. de Heer, and L. Forro, Solid State Commun. **99**, 513 (1996).
[46] S. Tasaki, K. Maekawa, and T. Yamabe, Phys. Rev. B **57**, 9301 (1998).
[47] I. Maeng, C. Kang, S. J. Oh, J.-H. Son, K. H. An, and Y. H. Lee, Appl. Phys. Lett. **90**, 051914 (2007).
[48] E. M. Furst and A. P. Gast, Phys. Rev. E **61**, 6732 (2000).
[49] R. T. Bonnecaze and J. F. Brady, J. Rheol. **36**, 73 (1992).
[50] More strictly, when $E_{\mathrm{chain}} \lesssim E_{\mathrm{align}}$ and the applied field is equal to E_{chain}, chains whose time-averaged axis direction is aligned with the applied field may form. The reason is that in this case, the nanotubes do not deviate much from being aligned with the applied field.